Advances in Materials Research, *Vol. 5, No. 2 (2016) 107-120*
DOI: http://dx.doi.org/10.12989/amr.2016.5.2.107

A novel higher order shear deformation theory based on the neutral surface concept of FGM plate under transverse load

Tahar Hassaine Daouadji*[1,3], Rabia Benferhat[2] and Belkacem Adim[1,3]

[1]*Departement de génie civil, University Ibn Khaldoun Tiaret, BP 78 Zaaroura, 14000 Tiaret, Algerie*
[2]*Laboratoire de Géomatériaux, Departement de Génie Civil, University de Chlef, Algerie*
[3]*Laboratoire de Géomatique et Développement Durable, University Ibn Khaldoun de Tiaret, Algerie*

(Received July 25, 2016, Revised August 31, 2016, Accepted October 7, 2016)

Abstract. The static analysis of the simply supported functionally graded plate under transverse load by using a new sinusoidal shear deformation theory based on the neutral surface concept is investigated analytically in the present paper. No transversal shear correction factors are needed because a correct representation of the transversal shearing strain is given. The mechanical properties of the FGM plate are assumed to vary continuously through the thickness according to a power law formulation except Poisson's ratio, which is kept constant. The equilibrium and stability equations are derived by employing the principle of virtual work. Results are provided for thick to thin plates and for different values of the gradient index k, which subjected to sinusoidal or uniformly distributed lateral loads. The accuracy of the present results is verified by comparing it with finite element solution. From the obtained results, it can be concluded that the proposed theory is accurate and efficient in predicting the displacements and stresses of functionally graded plates.

Keywords: functionally graded material; analytical solution; static analysis; neutral surface concept; power law formulation

1. Introduction

The idea of the construction of functionally graded materials (FGMs) was first introduced in 1984 by a group of Japanese materials scientists (Koizumi 1993). The accomplishment of functionally graded material is the realization of contemporary and distinct functions that cannot be achieved by the traditional composite materials. These are advanced composite materials with a microscopically inhomogeneous anatomy and are usually made from a mixture of ceramic and metal using powder metallurgy techniques. Different properties change continuously according to the variations in constituent volume fractions and these continuous changes in microstructure induce chemical, material, and micro structural gradient (Rabbach *et al*. 2000). The advantage of using this material is that it eliminates the interface problem due to smooth and continuous change of material properties from one surface to other.

They have many gained applications in rocket engine components, space plan body, nuclear

*Corresponding author, Professor, E-mail: daouadjitahar@gmail.com

http://www.techno-press.org/?journal=amr&subpage=7 ISSN: 2234-0912 (Print), 2234-179X (Online)

reactor components, first wall of fusion reactor, engine components, turbine blades, hip implant and other engineering and technological applications (Miyamoto 1999). Plates are employed in a wide range of mechanical and structural system components in civil, mechanical and aeronautical engineering. Liew *et al*. (2001) and Hamidi *et al*. (2015) studied the active control of functionally gradient material FGM plates with integrated piezoelectric sensor/actuator layers subjected to a thermal gradient using finite element formulation based on a first order shear deformation theory FSDT (Reddy 2000). Singha *et al*. (2011) have also presented asymmetric free vibration characteristics and thermoelastic stability of functionally graded plates using finite element procedure, Temperature field is assumed to be a uniform distribution over the plate surface and varied in thickness direction only (Abdelhak *et al*. 2015). Singha *et al*. (2011) and Bennoun *et al*. (2016) examined the nonlinear behaviors of functionally graded material (FGM) plates under transverse distributed load using a high precision plate bending finite element, the formulation is developed based on the first-order shear deformation theory (Benferhat 2015) considering the physical/exact neutral surface position. Hebali *et al*. (2014) and Bellifa *et al*. (2016), studied the static behavior of functionally graded rectangular plates based on his third-order shear deformation plate theory. Chi *et al*. (2006) carried out Mechanical behavior of functionally graded material plates under transverse load; the numerical solutions are evaluated directly from theoretical formulations and calculated by finite element method using MARC program. Zenkour (2006) has been investigated the static response of FG plate based on the middle surface using a generalized shear deformation theory with five unknown functions (Mahi 2015, Al-Basyoui 2015, Belabed 2014, Bourada 2015, Bouderba 2013, Bousahla 2014, Bounoura 2016). Kitipornchai *et al*. (2004) carried out the nonlinear vibration of imperfect shear deformable laminated rectangular plates comprising a homogeneous substrate and two layers of functionally graded materials FGMs (Ait Yahia *et al*. 2015), a semi-analytical method, which makes use of the one-dimensional differential quadrature method, the Galerkin technique, and an iteration process, is used to obtain the vibration frequencies for plates with various boundary conditions (Ait amar *et al*. 2014).

This paper aims to develop a new refined shear deformation plate theory for the static analysis of the FG plates under transverse load based on the neutral surface concept using analytical solution procedure. This theory does not require shear correction factors and just four unknown displacement functions are used against five or more unknown displacement functions used in the corresponding ones. The governing equations of equilibrium are derived from the principle of virtual displacements and Navier solutions for flexure of FG simply supported plates are presented. Convergence tests and comparison studies have been carried out to establish the accuracy and efficiency of the present results by comparing it with finite element solution of Singha *et al*. (2011). The variation of the displacements and stresses is highlighted for different thickness ratios, aspect ratios and volume fraction index for FGM plate subjected to sinusoidal and uniformly distributed load.

2. Geometric configuration and material properties

The FGM plate is regarded to be a single layer plate of uniform thickness. Here we ascertain the FGM plate of length a, width b and total thickness h made from anisotropic material of metal and ceramics, in which the composition varies from top to bottom surface. To specify the position of neutral surface of FG plates, two different planes are considered for the measurement of z, namely z_{ms} and z_{ns} measured from the middle surface and the neutral surface of the plate,

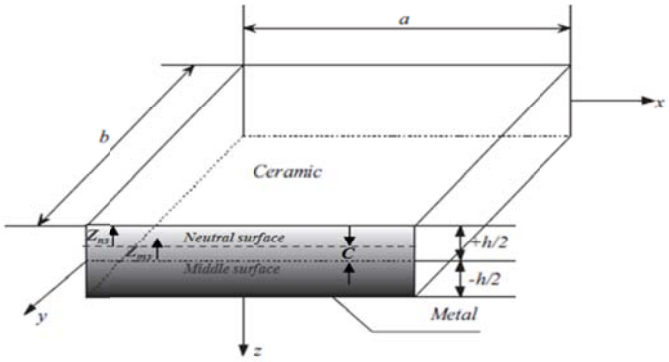

Fig. 1 Geometry and dimensions of the plate

respectively as shown in Fig. 1.

The volume fraction of ceramic (Vc) can be written in terms of z_{ms} and z_{ns} coordinates as (Praveen *et al*. 1998)

$$V_c(z) = \left(\frac{z_{ms}}{h} + \frac{1}{2}\right)^k = \left(\frac{z_{ns} + c}{h} + \frac{1}{2}\right)^k \tag{1}$$

Where h is the thickness of the plate and k denotes the power of FGM which takes values greater than or equal to zero. Also, the parameter C is the distance of neutral surface from the middle surface. The volume fraction of metal is expressed as

$$V_m(z) = 1 - V_c(z) \tag{2}$$

The effective Young's modulus E is expressed as

$$E(z) = E_m V_m(z) + E_c V_c(z) \tag{3}$$

Where E_m and E_c are the Young's modulus of the metal and ceramic respectively. The position of the neutral surface of the FG plate is determined to satisfy the first moment with respect to Young's modulus being zero as follows (Zhang *et al*. 2008, Singha *et al*. 2011)

$$\int_{-h/2}^{h/2} E(z_{ms})(z_{ms} - C)\,dz_{ms} = 0 \tag{4}$$

Consequently, the position of neutral surface can be obtained as

$$C = \frac{\int_{-h/2}^{h/2} E(z_{ms})\, z_{ms}\, dz_{ms}}{\int_{-h/2}^{h/2} E(z_{ms})\, dz_{ms}} \tag{5}$$

It can be seen that the physical neutral surface and the geometric middle surface are the same in

a homogeneous isotropic plate.

3. Displacement field and strains

In the present study, system of governing equations for FGM plate is derived by using variational approach. The origin of the material coordinates is at the neutral surface of the plate as shown in Fig. 1. The in-plane displacements and the transverse displacement for the plate is assumed as

$$\begin{aligned} u(x,y,z_{ns}) &= u_0(x,y) - z_{ns}\frac{\partial w_b}{\partial x} - f(z_{ns})\frac{\partial w_s}{\partial x} \\ v(x,y,z_{ns}) &= v_0(x,y) - z_{ns}\frac{\partial w_b}{\partial y} - f(z_{ns})\frac{\partial w_s}{\partial y} \\ w(x,y,z_{ns}) &= w_b(x,y) + w_s(x,y) \end{aligned} \tag{6}$$

Where $f(z_{ns})$ represents shape functions determining the distribution of the transverse shear strains and stresses along the thickness and is given as

$$f(z_{ns}) = z_{ns} + C - \sin\left(\frac{\pi(z_{ns}+C)}{h}\right) \tag{7}$$

It should be noted that unlike the first-order shear deformation theory, this theory does not require shear correction factors. The kinematic relations can be obtained as follows

$$\begin{aligned} \varepsilon_x &= \varepsilon_x^0 + z_{ns}\,k_x^b + f(z_{ns})\,k_x^s \\ \varepsilon_y &= \varepsilon_y^0 + z_{ns}\,k_y^b + f(z_{ns})\,k_y^s \\ \gamma_{xy} &= \gamma_{xy}^0 + z_{ns}\,k_{xy}^b + f(z_{ns})\,k_{xy}^s \\ \gamma_{yz} &= g(z_{ns})\,\gamma_{yz}^s \\ \gamma_{xz} &= g(z_{ns})\,\gamma_{xz}^s \\ \varepsilon_z &= 0 \end{aligned} \tag{8}$$

where

$$\begin{aligned} &\varepsilon_x^0 = \frac{\partial u_0}{\partial x}, \quad k_x^b = -\frac{\partial^2 w_b}{\partial x^2}, \quad k_x^s = -\frac{\partial^2 w_s}{\partial x^2} \\ &\varepsilon_y^0 = \frac{\partial v_0}{\partial y}, \quad k_y^b = -\frac{\partial^2 w_b}{\partial y^2}, \quad k_y^s = -\frac{\partial^2 w_s}{\partial y^2} \\ &\gamma_{xy}^0 = \frac{\partial u_0}{\partial y} + \frac{\partial v_0}{\partial x}, \quad k_{xy}^b = -2\frac{\partial^2 w_b}{\partial x \partial y}, \quad k_{xy}^s = -2\frac{\partial^2 w_s}{\partial x \partial y} \\ &\gamma_{yz}^s = \frac{\partial w_s}{\partial y}, \quad \gamma_{xz}^s = \frac{\partial w_s}{\partial x}, \quad g(z_{ns}) = 1 - f'(z_{ns}) \quad \text{and} \quad f'(z_{ns}) = \frac{df(z_{ns})}{dz_{ns}} \end{aligned} \tag{9}$$

The constitutive relation describes how the stresses and strains are related within the plate and

is expressed as

$$\begin{Bmatrix}\sigma_x\\ \sigma_y\\ \tau_{xy}\end{Bmatrix}=\begin{bmatrix}Q_{11} & Q_{12} & 0\\ Q_{12} & Q_{22} & 0\\ 0 & 0 & Q_{66}\end{bmatrix}\begin{Bmatrix}\varepsilon_x\\ \varepsilon_y\\ \gamma_{xy}\end{Bmatrix}$$
$$\begin{Bmatrix}\tau_{yz}\\ \tau_{zx}\end{Bmatrix}=\begin{bmatrix}Q_{44} & 0\\ 0 & Q_{55}\end{bmatrix}\begin{Bmatrix}\gamma_{yz}\\ \gamma_{zx}\end{Bmatrix} \tag{10}$$

where $(\sigma_x,\sigma_y,\tau_{xy},\tau_{xz},\tau_{yz})$ are the stress components; $(\varepsilon_x,\varepsilon_y,\gamma_{xy},\gamma_{xz},\gamma_{yz})$ are the strain components; Q_{ij} are the plane stress-reduced stiffnesses which can be calculated by

$$Q_{11}=Q_{22}=\frac{E(z_{ns})}{1-\nu^2}\qquad Q_{12}=\frac{\nu E(z_{ns})}{1-\nu^2}\qquad Q_{44}=Q_{55}=Q_{66}=\frac{E(z_{ns})}{2(1+\nu)} \tag{11}$$

3.1 Equilibrium equations

The equilibrium equations are derived by using the virtual work principle, which can be written for the plate as

$$\int_{-\frac{h}{2}-C}^{+\frac{h}{2}-C}\int_{\Omega}(\sigma_x\delta\varepsilon_x+\sigma_y\delta\varepsilon_y+\tau_{xy}\delta\gamma_{xy}+\tau_{yz}\delta\gamma_{yz}+\tau_{xz}\delta\gamma_{xz}).d\Omega.dz-\int_{\Omega}q.\delta w.d\Omega=0 \tag{12}$$

where Ω is the top surface and q is the applied transverse load.

Substituting Eqs. (9) and (10) into Eq. (12) and integrating through the thickness of the plate, Eq. (12) can be rewritten as

$$\begin{aligned}&\int_{\Omega}(N_x.\delta\varepsilon_x^0{}_{+x}+N_y.\delta\varepsilon_y^0+N_{xy}.\delta\gamma_{xy}^0+M_x^b.\delta k_x^b+M_y^b.\delta k_y^b+M_{xy}^b.\delta k_{xy}^b+M_x^s.\delta k_x^s\\&+M_y^s.\delta k_y^s+M_{xy}^s.\delta k_{xy}^s+S_{yz}^s.\delta\gamma_{yz}^s+S_{xz}^s.\delta\gamma_{xz}^s)d\Omega-\int_{\Omega}q(\delta w+\delta w_b)d\Omega=0\end{aligned} \tag{13}$$

where

$$\begin{Bmatrix}N_x, & N_y, & N_{xy},\\ M_x^b, & M_y^b, & M_{xy}^b,\\ M_x^s, & M_y^s, & M_{xy}^s,\end{Bmatrix}=\int_{-\frac{h}{2}-C}^{+\frac{h}{2}-C}(\sigma_x,\sigma_y,\tau_{xy})\begin{Bmatrix}1\\ z\\ f(z_{ns})\end{Bmatrix}dz_{ns} \tag{14}$$

$$(S_{xz}^s,S_{yz}^s)=\int_{-\frac{h}{2}-C}^{+\frac{h}{2}-C}(\tau_{xz},\tau_{yz})g(z_{ns})dz_{ns} \tag{15}$$

The governing equations of equilibrium can be derived from Eq. (16) by integrating the displacement gradients by parts and setting the coefficients δu_0, δv_0, δw_b, and δw_s zero separately. Thus, one can obtain the equilibrium equations associated with the present shear deformation theory

$$\begin{cases} \delta u : \dfrac{\partial N_x}{\partial x} + \dfrac{\partial N_{xy}}{\partial y} = 0 \\ \delta v : \dfrac{\partial N_{xy}}{\partial x} + \dfrac{\partial N_y}{\partial y} = 0 \\ \delta w_b : \dfrac{\partial^2 M_x^b}{\partial x^2} + 2\dfrac{\partial^2 M_{xy}^b}{\partial x \partial y} + \dfrac{\partial^2 M_y^b}{\partial y^2} + q = 0 \\ \delta w_s : \dfrac{\partial^2 M_x^s}{\partial x^2} + 2\dfrac{\partial^2 M_{xy}^s}{\partial x \partial y} + \dfrac{\partial^2 M_y^s}{\partial y^2} + \dfrac{\partial S_{xz}^s}{\partial x} + \dfrac{\partial S_{yz}^s}{\partial y} + q = 0 \end{cases} \tag{16}$$

Using Eq. (10) in Eq. (14), the stress resultants of a plate can be related to the total strains by

$$\begin{Bmatrix} N \\ M^b \\ M^s \end{Bmatrix} = \begin{bmatrix} A & B & B^s \\ A & D & D^s \\ B^s & D^s & H^s \end{bmatrix} \begin{Bmatrix} \varepsilon \\ k^b \\ k^s \end{Bmatrix} \tag{17}$$

$$; \qquad S = A^s \gamma$$

Where

$$N = \left\{N_x, N_y, N_{xy}\right\}^t, \qquad M^b = \left\{M_x^b, M_y^b, M_{xy}^b\right\}^t, \qquad M^s = \left\{M_x^s, M_y^s, M_{xy}^s\right\}^t \tag{18}$$

$$\varepsilon = \left\{\varepsilon_x^0, \varepsilon_y^0, \varepsilon_{xy}^0\right\}^t, \qquad k^b = \left\{k_x^b, k_y^b, k_{xy}^b\right\}^t, \qquad k^s = \left\{k_x^s, k_y^s, k_{xy}^s\right\}^t \tag{19}$$

$$A = \begin{bmatrix} A_{11} & A_{12} & 0 \\ A_{12} & A_{22} & 0 \\ 0 & 0 & A_{66} \end{bmatrix}, \qquad B = \begin{bmatrix} B_{11} & B_{12} & 0 \\ B_{12} & B_{22} & 0 \\ 0 & 0 & B_{66} \end{bmatrix}, \qquad D = \begin{bmatrix} D_{11} & D_{12} & 0 \\ D_{12} & D_{22} & 0 \\ 0 & 0 & D_{66} \end{bmatrix} \tag{20}$$

$$B^s = \begin{bmatrix} B_{11}^s & B_{12}^s & 0 \\ B_{12}^s & B_{22}^s & 0 \\ 0 & 0 & B_{66}^s \end{bmatrix}, \qquad D^s = \begin{bmatrix} D_{11}^s & D_{12}^s & 0 \\ D_{12}^s & D_{22}^s & 0 \\ 0 & 0 & D_{66}^s \end{bmatrix}, \qquad H^s = \begin{bmatrix} H_{11}^s & H_{12}^s & 0 \\ H_{12}^s & H_{22}^s & 0 \\ 0 & 0 & H_{66}^s \end{bmatrix} \tag{21}$$

$$S = \left\{S_{xz}^z, S_{yz}^s\right\}^t, \qquad \gamma = \left\{\gamma_{xz}, \gamma_{yz}\right\}^t, \qquad A^s = \begin{bmatrix} A_{44}^s & 0 \\ 0 & A_{55}^s \end{bmatrix} \tag{22}$$

The stiffness coefficients A_{ij} and B_{ij}, etc., are defined as

$$\begin{Bmatrix} A_{11} & B_{11} & D_{11} & B_{11}^s & D_{11}^s & H_{11}^s \\ A_{12} & B_{12} & D_{12} & B_{12}^s & D_{12}^s & H_{12}^s \\ A_{66} & B_{66} & D_{66} & B_{66}^s & D_{66}^s & H_{66}^s \end{Bmatrix} = \int_{-\frac{h}{2}-C}^{+\frac{h}{2}-C} Q_{11}(1, z_{ns}^{\,2}, f(z_{ns}), z_{ns} f(z_{ns}), f^2(z_{ns})) \begin{Bmatrix} 1 \\ \nu \\ \frac{1-\nu}{2} \end{Bmatrix} dz_{ns} \tag{23}$$

$$(A_{22}, B_{22}, D_{22}, B_{22}^s, D_{22}^s, H_{22}^s) = (A_{11}, B_{11}, D_{11}, B_{11}^s, D_{11}^s, H_{11}^s), \quad Q_{11} = \frac{E(z_{ns})}{1-\mu^2} \tag{24}$$

$$A_{44}^s = A_{55}^s = \int_{-\frac{h}{2}-C}^{+\frac{h}{2}-C} \frac{E(z_{ns})}{2(1+\nu)} [g(z_{ns})]^2 \, dz_{ns} \tag{25}$$

Substituting from Eq. (14) into Eq. (16), we obtain the following equation

$$\begin{aligned} &A_{11} d_{11} u_0 + A_{66} D_{22} u_0 + (A_{12} + A_{66}) d_{12} v_0 - B_{11} d_{11} w_b - (B_{12} + 2B_{66}) d_{122} w_b \\ &- (B_{12}^s + 2B_{66}^s) d_{122} w_s - B_{11}^s d_{111} w_s = 0 \end{aligned} \tag{26}$$

$$\begin{aligned} &A_{22} d_{22} v_0 + A_{66} d_{11} v_0 + (A_{12} + A_{66}) d_{12} u_0 - B_{22} d_{222} w_b - (B_{12} + 2B_{66}) d_{112} w_b \\ &- (B_{12}^s + 2B_{66}^s) d_{112} w_s - B_{22}^s d_{222} w_s = 0 \end{aligned} \tag{27}$$

$$\begin{aligned} &B_{11} d_{111} u_0 + (B_{12} + 2B_{66}) d_{122} u_0 + (B_{12} + 2B_{66}) d_{112} v_0 + B_{22} d_{222} v_0 - D_{11} d_{1111} w_b \\ &- 2(D_{12} + 2D_{66}) d_{1122} w_b - D_{22} d_{2222} w_b - D_{11}^s d_{1111} w_s - 2(D_{12}^s + 2D_{66}^s) d_{1122} w_s \\ &- D_{22}^s d_{2222} w_s + q = 0 \end{aligned} \tag{28}$$

$$\begin{aligned} &B_{11}^s d_{111} u_0 + (B_{12}^s + 2B_{66}^s) d_{122} u_0 + (B_{12}^s + 2B_{66}^s) d_{112} v_0 + B_{22}^s d_{222} v_0 - D_{11}^s d_{1111} w_b \\ &- 2(D_{12}^s + 2D_{66}^s) d_{1122} w_b - D_{22}^s d_{2222} w_b - H_{11}^s d_{1111} w_s - 2(H_{12}^s + 2H_{66}^s) d_{1122} w_s \\ &- H_{22}^s d_{2222} w_s + A_{55}^s d_{11} w_s + A_{44}^s d_{22} w_s + q = 0 \end{aligned} \tag{29}$$

where d_{ij}, d_{ijl}, and d_{ijlm} are the following differential operators

$$d_{ij} = \frac{\partial^2}{\partial x_i \partial x_j}, \quad d_{ijl} = \frac{\partial^3}{\partial x_i \partial x_j \partial x_l}, \quad d_{ijlm} = \frac{\partial^4}{\partial x_i \partial x_j \partial x_l \partial x_m}, \quad (i, j, l, m = 1, 2) \tag{30}$$

4. Numerical results and discussion

In this section, various numerical examples are presented and discussed to verify the accuracy of present theory in predicting the bending of simply supported FG plates under distributed transverse load is taken up for investigation. For numerical results, an Al/Al_2O_3 plate composed of aluminium (as metal) and alumina (as ceramic) is considered. The material properties assumed in

the present analysis are as follows:

Ceramic (P_C : Alumina, Al_2O_3): $E_c = 380$ GPa; $\rho_c = 5700 kg/m^3$

Metal (P_M : Aluminium, Al): $E_m = 70$ GPa; $\rho_m = 2702 kg/m^3$

Poisson's ratio is 0.3 for both alumina and aluminium. And their properties change through the thickness of the plate according to power-law. The bottom surfaces of the FG plate are aluminium rich, whereas the top surfaces of the FG plate are alumina rich.

The boundary conditions considered here are as follows: Immovable simply supported: $u_0=v_0=w=0$ on the neutral surface edges

The coefficients $\boldsymbol{q_{mn}}$ in the case of a uniformly distributed load are

$$q_{mn} = \begin{cases} \dfrac{16\, q_0}{mn\,\pi^2} & \text{for odd } m \text{ and } n \\ 0 & \text{for even } m \text{ and } n \end{cases} \tag{31}$$

Where q_0 is the intensity of the load at the plate center. In the case of a sinusoidally distributed load, we have (with *:* $m=n=1$ and $q_{11}=q_0$.)

$$q(x,y) = q_0 \sin\left(\frac{\pi x}{a}\right)\sin\left(\frac{\pi y}{b}\right) \tag{32}$$

For verification purpose, the obtained results are compared with those predicted using finite element solutions of Singha *et al*. (2011). In all examples, no transversal shear correction factors are used because a correct representation of the transversal shearing strain is given. For convenience, the following nondimensionalizations and the stresses are used in presenting the numerical results in graphical and tabular form

$$\bar{w} = 10\,\frac{E_C h^3}{q_0 a^4} w\left(\frac{a}{2},\frac{b}{2}\right), \quad \bar{u} = 100\,\frac{E_C h^3}{q_0 a^4} u\left(0,\frac{b}{2},\frac{-h}{4} - C\right),$$

$$\bar{v} = 100\,\frac{E_C h^3}{q_0 a^4} v\left(\frac{a}{2},0,\frac{-h}{6} - C\right)$$

$$\overline{\sigma_x} = \frac{h}{hq_0}\sigma_x\left(\frac{a}{2},\frac{b}{2},\frac{h}{2} - C\right), \quad \overline{\sigma_y} = \frac{h}{hq_0}\sigma_y\left(\frac{a}{2},\frac{b}{2},\frac{h}{3} - C\right), \tag{33}$$

$$\overline{\tau_{xy}} = \frac{h}{hq_0}\tau_{xy}\left(0,0,-\frac{h}{3} - C\right)$$

$$\overline{\tau_{xz}} = \frac{h}{hq_0}\tau_{xz}\left(0,\frac{b}{2},-C\right), \quad \overline{\tau_{yz}} = \frac{h}{hq_0}\tau_{yz}\left(\frac{a}{2},0,\frac{h}{6} - C\right).$$

To illustrate the accuracy of present theory for wide range of power law index k and thickness ratio a/h, the variations of Non-dimensional central displacement and stresses are illustrated in Table 1 and Table 2.

Table 1 shows the comparison of Non-dimensional central displacement and the maximum shear stress of simply supported thin (a/h=100) square alumina/aluminum FGM plate under uniformly distributed load obtained by present theory with those given by Singha *et al*. (2011). It can be seen that the proposed refined theory using analytical solution based on the neutral surface

Table 1 Comparison study of Non-dimensional central displacement and the maximum shear stress of simply supported thin (a/h=100) square alumina/aluminum FGM plate under uniformly distributed load (q_0)

Volume fraction index k	Theory	Shift of neutral surface C	Shear correction factor	$\overline{w}$	$\overline{\tau_{xz}}$
Ceramic	Singha (2011) Model	0	0.83333	0.004064	0.50699
	Present Model	0	/	0.004064	0.51644
0,5	Singha (2011) Model	0.0747	0.84515	0.006269	0.53114
	Present Model	0.0747	/	0.006269	0.52799
1	Singha (2011) Model	0.1148	0.82921	0.008154	0.54043
	Present Model	0.1148	/	0.008154	0.51714
1,5	Singha (2011) Model	0.1370	0.80016	0.009525	0.53804
	Present Model	0.1370	/	0.009525	0.49742
2	Singha (2011) Model	0.1490	0.76778	0.010449	0.53039
	Present Model	0.1490	/	0.010449	0.47644
3	Singha (2011) Model	0.1576	0.71661	0.011482	0.51386
	Present Model	0.1576	/	0.011482	0.44339
5	Singha (2011) Model	0.1517	0.67677	0.012359	0.49427
	Present Model	0.1517	/	0.012359	0.42445
10	Singha (2011) Model	0.1196	0.1196	0.013569	0.47897
	Present Model	0.1517	0.67677	0.012359	0.49427
Metal	Singha (2011) Model	0	0.83333	0.022064	0.50699
	Present Model	0	/	0.022064	0.51644

Table 2 Comparison study of Non-dimensional central displacement and in- plane stress of thick square (a/h=10) alumina/ aluminum FGM plates under uniformly distributed (q_0) and sinusoidal loads

Volume fraction index k	$\overline{w}$		$\overline{\sigma_{xx}}$	
	Singha (2011) Model	Present Model	Singha (2011) Model	Present Model
Uniformly distributed load				
Ceramic (k=0)	0.4666	0.4665	2.8688	2.8932
k=1	0.9290	0.9287	4.4303	4.4499
k=2	1.1952	1.1936	5.1689	5.1737
k=4	1.3908	1.3952	5.8035	5.8132
Metal (k=∞)	2.5327	2.5326	2.8687	2.8932
Lateral sinusoidal load				
Ceramic (k=0)	0.2961	0.2960	1.9679	1.9955
k=1	0.5891	0.5889	3.0389	3.1212
k=2	0.7582	0.7575	3.5456	3.6720
k=4	0.8831	0.8822	3.9813	4.1647
Metal (k=∞)	1.6072	1.6070	1.9679	1.9955

concept and finite element solution give identical results of non-dimensional central displacement as well as maximum shear stress for all values of power law index k. It is observed that the physical neutral surface and the geometric middle surface are the same (C=0) in a homogeneous isotropic plate and takes maximum values (C=0.1579) when the power low index k is equal to 3.3. Is to be mentioned that the results are obtained without using shear correction factors because a correct representation of the transversal shearing strain.

The capability of the present solution is also tested for the non-dimensional central displacement and in-plane stress of thick square (a/h=10) alumina/aluminum FGM plates under uniformly distributed and sinusoidal loads in Table 2. Close correlation is achieved. It is important to observe that the uniform load distribution always over predicts the displacements and stresses magnitude; also the stresses for a fully ceramic plate are the same as that for a fully metal plate. This is because the plate for these two cases is fully homogeneous and the stresses do not depend on the modulus of elasticity.

Table 3 examines the effect of volume fraction exponent on the dimensionless stresses and displacements of a FGM rectangular plate (b=2a) subjected to uniform distributed loads with two values of side to thickness ratio (a/h=4, 10). This effect is much more pronounced when volume fraction index k increase and the plate becomes thinner. It is seen from Table 3 that as the value of the power-law exponent k increases, the deflections of the plate increase. This is due to the fact that an increase in the power-law exponent yields an increase in the bending rigidity of the plate. Results in Table 3 should serve as benchmark results for future comparisons.

Fig. 2 contains the plots of the non dimensional central deflection for thick to thin rectangular (b=2a) FGM plate subjected to uniform distributed load versus power law index k (k=0 to 5). It is clear that the increase of the power law index k causes an increase of the non dimensional central deflection. Figs. 3 and 4 shows the variation of the non-dimensional deflexion for the rectangular (b=2a) FGM plate under uniform load as function as the aspect and side-to-thickness ratio, respectively. It can be observed that deflection of metal rich composition is more when compared to ceramic rich Al/Al_2O_3 FGM plate. This can be accounted for the Young's modulus of ceramic (E_c=380 GPa) being high when compared to that of metal (E_m=70 GPa).

Figs. 5 and 6 illustrates the distribution of normal stresses of the FGM plate (b=2a and k=2) with different values of side-to-thickness ratio. As expected the normal stresses are compressive on the ceramic rich face (top) and tensile on the metal rich face (bottom). Note that the plots read negative sign for tensile stresses and positive sign for compressive stresses. Figs. 7 to 9 displays the shear stresses of the FGM plate through the thickness. The volume fraction exponent of the FGM plate is taken as k=2 in this figures. As seen from Fig. 7, the longitudinal tangential stress τ_{xy} takes maximum values on the top and bottom surfaces of the rectangular (b=2a) FGM plate. It is observed from the Figs. 8 and 9 that, the shear stress τ_{xz}, τ_{yz} across plate thickness is symmetric about the neutral axis, this last upwards towards the ceramic rich face.

Table 3 Effects of volume fraction exponent and side to thickness ratio on the dimensionless stresses and displacements of a FGM rectangular plate (b=2a) under uniformly distributed loads

Volume fraction index k	Side to thickness ratio a/h	$\overline{w}$	$\overline{\sigma_x}$	$\overline{\sigma_y}$	$\overline{\tau_{yz}}$	$\overline{\tau_{xz}}$	$\overline{\tau_{xy}}$
Ceramic	4	1.3272	2.5108	0.7341	0.4723	0.6946	0.7103
	10	1.1415	6.1293	1.8510	0.4822	0.7086	1.8362

Table 3 Continued

Volume fraction index *k*	Side to thickness ratio a/h	$\overline{w}$	$\overline{\sigma_x}$	$\overline{\sigma_y}$	$\overline{\tau_{yz}}$	$\overline{\tau_{xz}}$	$\overline{\tau_{xy}}$
1	4	2.5574	2.2478	0.6771	0.5118	1.1141	0.6200
	10	2.2777	8.7001	2.0404	0.5164	0.4856	1.5781
2	4	3.4854	7.6716	1.0511	0.7394	1.1865	0.5418
	10	2.9234	9.4198	2.1137	0.6144	0.4147	1.3831
3	4	3.7858	4.3999	0.9826	0.4976	0.2696	0.8317
	10	3.2287	12.0859	1.8312	0.6121	0.6248	1.4275
4	4	4.0311	5.2096	0.6277	0.5409	0.6432	0.5177
	10	3.3857	11.3239	1.6200	0.5081	0.7823	1.4672
5	4	4.5673	12.9306	1.1386	0.1759	1.5095	0.4390
	10	3.4935	11.8503	1.4842	0.5119	0.7141	1.4906
6	4	4.6281	12.1421	0.8783	0.6433	1.2443	0.5656
	10	3.5825	13.2704	1.4593	0.5048	0.5877	1.5007
7	4	4.5253	7.2964	0.6285	0.5353	0.7264	0.5625
	10	3.6611	15.7895	1.1875	0.6068	0.7144	1.4479
8	4	4.6137	7.6834	0.5054	0.5056	0.6217	0.5744
	10	3.7308	15.3374	1.3719	0.4816	0.6867	1.5109
9	4	4.6704	6.6490	0.5657	0.4935	0.6508	0.5670
	10	3.7962	15.8030	1.3063	0.4762	0.5830	1.5153
10	4	4.6959	5.0397	0.5147	0.3694	0.8498	0.5655
	10	3.8548	14.3419	1.2419	0.4293	0.6689	1.5278
Metal	4	7.2051	2.5108	0.7341	0.4723	0.6946	0.7103
	10	6.1967	6.1293	1.8510	0.4822	0.7086	1.8362

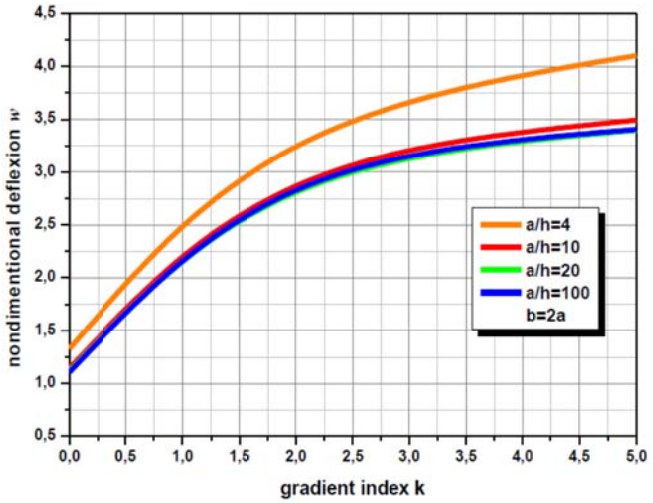

Fig. 2 Nondimensional central deflection across power law index *k*

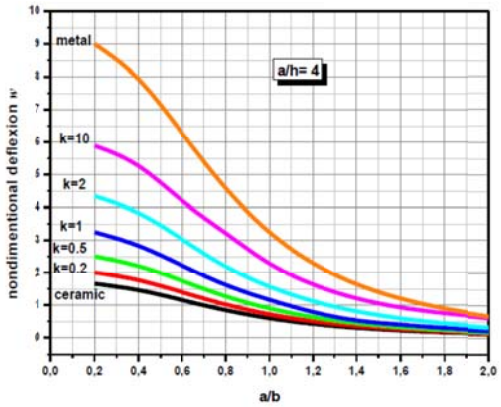

Fig. 3 Nondimensional central deflection across the aspect ratio (a/b)

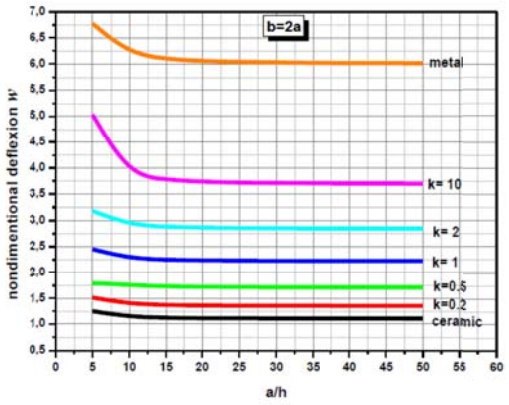

Fig. 4 Nondimensional central deflection across the side to thickness ratio (a/h)

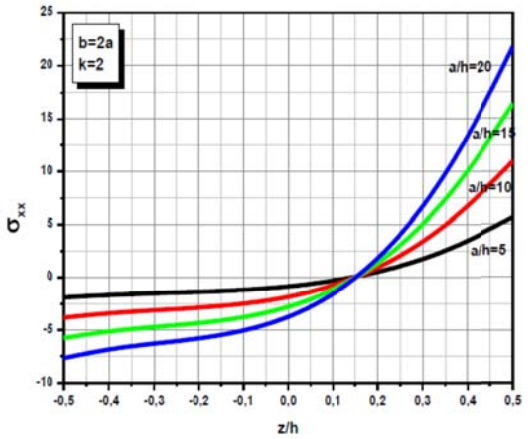

Fig. 5 In plane longitudinal stresses σxx across the thickness

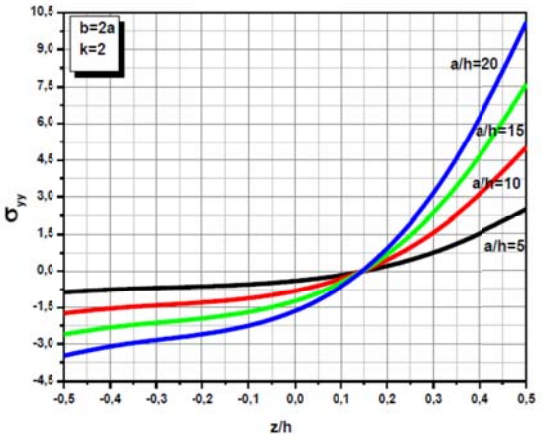

Fig. 6 In plane longitudinal stresses σ_{yy} across the thickness

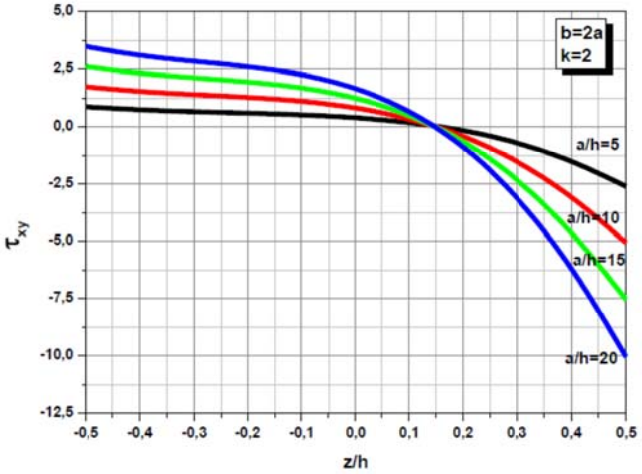

Fig. 7 In plane shear stresses τ_{xy} across the thickness

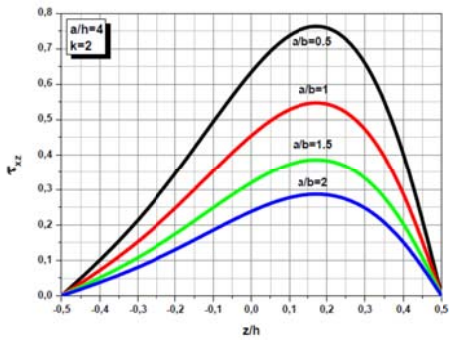

Fig. 8 Transverse shear stresses τ_{xz} across the thickness

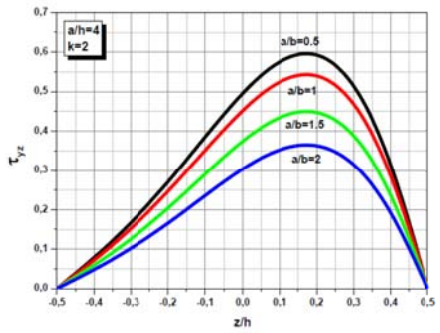

Fig. 9 Transverse shear stresses τ_{yz} across the thickness

5. Conclusions

In this work, an efficient new refined shear deformation theory based on the neutral surface concept was effectively used to study extensively the static analysis of an FG simply-supported plate under distributed transverse loads using analytical procedure. The theory gives a parabolic distribution of the transverse shear strains and satisfies the zero traction boundary conditions on the surfaces of the plate without using shear correction factors. Poisson's ratio is assumed to be a constant, and Young's modulus is assumed to vary in power law fashion through the thickness. Non-dimensional stresses and displacements are computed for plates with ceramic-metal mixture. The results presented here clearly demonstrate that the present theory agreed well with the finite element solutions

Acknowledgments

The authors thank the referees for their valuable comments.

References

Abdelhak, Z., Hadji, L. and Hassaine Daouadji, T. (2015), "Thermal buckling of functionally graded plates using a n-order four variable refined theory", *Adv. Mater. Res.*, **4**(1), 31-44.

Ait Amar Meziane, M., Abdelaziz, H.H. and Tounsi, A. (2014), "An efficient and simple refined theory for buckling and free vibration of exponentially graded sandwich plates under various boundary conditions", *J. Sandwich Struct. Mater.*, **16**(3), 293-318.

Ait Yahia, S., Ait Atmane, H. and Tounsi, A. (2015), "Wave propagation in functionally graded plates with porosities using various higher-order shear deformation plate theories", *Struct. Eng. Mech.*, **53**(6), 1143-1165.

Al-Basyouni, K.S., Tounsi, A. and Mahmoud, S.R. (2015), "Size dependent bending and vibration analysis of functionally graded micro beams based on modified couple stress theory and neutral surface position", *Compos. Struct.*, **125**, 621-630.

Bellifa, H., Benrahou, K.H. and Tounsi, A. (2016), "Bending and free vibration analysis of functionally graded plates using a simple shear deformation theory and the concept the neutral surface position", *J.*

Braz. Soc. Mech. Sci. Eng., **38**(1), 265-275.
Belabed, Z., Houari, M.S.A., Tounsi, A., Mahmoud, S.R. and Anwar Bég, O. (2014), "An efficient and simple higher order shear and normal deformation theory for functionally graded material FGM plates", *Composites: Part B*, **60**, 274-283.
Benferhat, R., Hassaine Daouadji, T. and Said Mansour, M. (2015), "A higher order shear deformation nodel for bending analysis of functionally graded plates", *Trans. Indian Inst. Metals*, **68**(1), 7-16.
Bennoun, M. and Tounsi, A. (2016), "A novel five variable refined plate theory for vibration analysis of functionally graded sandwich plates", *Mech. Adv. Mater. Struct.*, **23**(4), 423-431.
Bouderba, B., Houari, M.S.A. and Tounsi, A. (2013), "Thermomechanical bending response of FGM thick plates resting on Winkler-Pasternak elastic foundations", *Steel Compos. Struct.*, **14**(1), 85-104.
Bounouara, F., Benrahou, K.H., Belkorissat, I. and Tounsi, A. (2016), "A nonlocal zeroth-order shear deformation theory for free vibration of functionally graded nanoscale plates resting on elastic foundation", *Steel Compos. Struct.*, **20**(2), 227-249.
Bourada, M., Kaci, A., Houari, M.S.A. and Tounsi, A. (2015), "A new simple shear and normal deformations theory for functionally graded beams", *Steel Compos. Struct.*, **18**(2), 409-423.
Bousahla, A.A., Houari, M.S.A., Tounsi, A. and Adda Bedia, E.A. (2014), "A novel higher order shear and normal deformation theory based on neutral surface position for bending analysis of advanced composite plates", *Int. J. Comput. Method*., **11**(6), 1350082.
Chi, S.H. and Chung, Y.L. (2006), "Mechanical behavior of functionally graded material plates under transverse load-Part II: Numerical results", *Int. J. Solid. Struct.*, **43**, 3675-3691.
Hamidi, A., Mahmoud, S.R. and Tounsi, A. (2015), "A sinusoidal plate theory with 5- unknowns and stretching effect for thermomechanical bending of functionally graded sandwich plates", *Steel Compos. Struct*., **18**(1), 235-253.
Hebali, H., A. Tounsi, S. Houari and E.A. Adda Bedia (2014), "A new quasi-3D hyperbolic shear deformation theory for the static and free vibration analysis of functionally graded plate", *J. Eng. Mech.*, ASCE, **140**(2), 374-383.
Kitipornchai, S., Yang, J. and Liew, K.M. (2004), "Semi-analytical solution for nonlinear vibration of laminated FGM plates with geometric imperfections", *Int. J. Solid Struct*., **41**(9), 2235-2257.
Koizumi, M. (1993), "The concept of FGM", *Ceramic Trans. Funct. Grad. Mater.*, **34**, 3-10.
Liew, K.M., He, X.Q., Ng, T. and Sivashanker, S. (2001), "Active control of FGM plates subjected to a temperature gradient: Modelling via finite element method based on FSDT", *Int. J. Numer. Meth. Eng*., **52**(11), 1253-1271.
Mahi, A., E. Adda Bedia and A. Tounsi (2015), "A new hyperbolic shear deformation theory for bending and free vibration analysis of isotropic, functionally graded, sandwich and laminated composite plate", *Appl. Math. Model.*, **39**(9), 2489-2508.
Miyamoto, Y., Kaysser, W.A., Rabin, B.H. and Ford, R.G. (1999), *Functionally graded materials: design, processing and applications*, London: Kluwer Academic Publishers.
Praveen, G.N. and Reddy, J.N. (1998), "Nonlinear transient thermoelastic analysis of functionally graded ceramic-metal plates", *Int. J. Solid. Struct*., **35**(33), 4457-4476.
Rabbach, S. and Lehnert, W. (2000), "Investigations of deformation of FGM", *Comput. Mater. Sci.*, **19**(1), 298-303.
Reddy, J. (2000), "Analysis of functionally graded plates", *Int. J. Numer. Method. Eng*., **47**(1-3), 663-684.
Singha, M.K., Prakash, T. and Ganapathi, M. (2011), "Finite element analysis of functionally graded plates under transverse load", *Finite Element. Anal. Des*., **47**(4), 453-460.
Zenkour, A.M. (2006), "Generalized shear deformation theory for bending analysis of functionally graded plates", *Appl. Math. Model*., **30**(1), 67-84.
Zhang, D.G. and Zhou, Y. (2008), "A theoretical analysis of FGM thin plates based on physical neutral surface", *Comput. Mater. Sci*., **44**(2), 716-720.